Korean J. Chem. Eng., 35(6), 1365-1372 (2018)
DOI: 10.1007/s11814-018-0041-9

pISSN: 0256-1115
eISSN: 1975-7220

Synthesis and characterization of decyl phosphonic acid, applications in emulsion polymerization and anti-corrosion coating

The-Anh Phan*, François-Xavier Perrin, and Lam Nguyen-Dinh*,†**

*The University of Danang, University of Science and Technology, Danang, Viet Nam
**Laboratoire MAPIEM EA 4323, SeaTech-Ecole d'ingénieurs, Université de Toulon, La Garde Cedex, France
(*Received 6 November 2017 • accepted 12 March 2018*)

Abstract−Alkyl phosphonic acids are amphiphilic structures consisting of non-polar organic hydrophobic groups and anionic inorganic hydrophilic groups, which makes them be able to behave as surfactants as well as smart corrosion inhibitors. A simple and high yield (up to 87%) pathway for synthesizing decyl phosphonic acid (DPA) is described. ^{1}H and ^{13}C-NMR) as well as FTIR spectroscopy were used to characterize chemical structures and purity of the obtained product. Thermal properties and crystal structure of DPA were investigated using differential scanning calorimetry analysis (DSC) and thermogravimetric analysis (TGA). The stability of DPA in Oil-in-Water (O/W) and Water-in-Oil (W/O) emulsions was improved in the presence of ammonium persulfate (APS), which allowed us to measure their specific characteristics such as particle size and zeta potential (ξ) of micelles. Both emulsions were used for synthesizing polyaniline (PANI) by emulsion polymerization. Wettability of DPA on the mild steel surface was examined using contact angle measurements. Moreover, corrosion-inhibition properties studied by using electrochemical impedance spectroscopy (EIS) technique and salt spray test results revealed that DPA can be an efficient ingredient for anti-corrosion coating.

Keywords: Surfactant, Oil-in-water Emulsion, Water-in-oil Emulsion, Polyaniline

INTRODUCTION

With a amphiphilic chemical structure consisting of both non-polar organic hydrophobic groups (R=alkyl or aryl) and anionic hydrophilic groups (-PO_3H_2), alkyl phosphonic acids (RPO_3H_2) can be considered as a surfactant with diprotic character arising from the two hydroxyl groups at the polar head. The charge of polar head groups can be varied from nearly zero to −2.

The geometry of hydrophilic head groups is nearly tetrahedral, which can act both as a hydrogen-bond donor via two P-OH groups and a hydrogen-bond acceptor through the P=O oxygen. Phosphonic acids possess strong hydrogen bonds, which are important characters widely used in the fields of biological activity such as potential antibiotics and enzyme inhibitors [1,2]. Furthermore the tridentate character of the PO_3H_2 group enables phosphonic acid to form self-assembled monolayers (SAMs) on metal surfaces [3-5]. SAMs have been intensively studied in recent years because they have wide applications in corrosion inhibition [6], sensors [7] and adhesion [8,9]. In comparison with carboxylic acids, phosphonic acids have stronger bonds with metal oxide surfaces [10]. The long-alkyl chains of the hydrophobic tail of phosphonic acids tend to form supramolecular structures [11,12] which in turn can enhance the anti-corrosion properties of the acids. Owing to the excellent bonding with the substrate through covalent chemical bonding, hydrogen bonding or acid-base interactions and the ability to act as a corrosion inhibiter, alkyl phosphonic acids are considered as effective alternatives for Cr (VI) based coatings [13].

Alkyl phosphonic acids have been synthesized by many different methods: (i) free radical addition of dialkylphosphonites [14], (ii) oxidation of phosphonous acids or their esters [15,16] or (iii) Arbuzov reaction of trialkylphosphites with suitable alkylation agents [7,17,18]. The free radical addition method showed a very low yield below 20% [14]. The yield can be improved by the oxidation method, for example, the oxidation of *n*-decylphosphonous acid in solution of $KMnO_4$ which produced an *n*-decylphosphonic acid with the yield of 49% [19]. Due to the simplicity and high yield, the Arbuzov reaction (method (iii)) is the most popular method to produce alkyl phosphonic acids. The syntheses of alkyl phosphonic acids such as mercaptoundecanylphosphonic acid [17], hexadecylphosphonic acid [18], 1,12-dodecanediyl bis(phosphonic acid) have been reported [5]. Chan et al. [20] described the decylphosphonic acid synthesis process, but did not mention the yield of the reaction.

On the basis of Michaelis-Arbuzov and Michaelis-Becker reactions, we have developed a method to synthesize decyl phosphonic acid (DPA) in two stages. This method improves DPA yield to 87%, which is twice larger than that of a previous work [19,21].

Our group has recently demonstrated the formation of anticorrosive coatings based on DPA doped polyaniline [22,23], in which, the DPA acted as both a surfactant and a smart corrosion inhibitor. Being one of ingredients of anti-corrosion paint, DPA released from the coating forms insoluble salts with iron ions and prevents further corrosion when a defect occurs on the coating either because of manufacturing or due to damage. However, the DPA synthesized process and characterizations of the original emulsion

†To whom correspondence should be addressed.
E-mail: ndlam@dut.udn.vn

systems have not yet been discussed. Therefore, this article focuses on the high-yield synthesis and characterization of DPA. In addition, the formation and properties of O/W and W/O emulsion systems using DPA as surfactant are also addressed for potential application in emulsion polymerization [22,23]. We used several characterization methods including nuclear magnetic resonance (NMR), Fourier transform infrared spectroscopy (FTIR), differential scanning calorimetry analysis (DSC), thermo-gravimetric analysis (TGA), X-ray diffraction (XRD), dynamic light scattering (DLS) and contact angle measurements. Electrochemical impedance spectroscopy (EIS) and salt spray tests were also conducted to evaluate the corrosion inhibition properties of DPA.

EXPERIMENTATION

1. Chemicals

1-Bromodecane, $C_{10}H_{21}Br$, (98% purity) and triethyl phosphite, $P(OEt)_3$, (98% purity) were purchased from Sigma-Aldrich. Hydrochloric acid, HCl, (37%) was obtained from Fluka. These chemicals were used to synthesize decyl phosphonic acid, DPA, in the Matériaux, Polymères, Interfaces, Environnement Marin laboratory (MAPIEM Lab). Chloroforme, $CHCl_3$, (≥99.5% purity), magnesium sulfate anhydrous, $MgSO_4$, (≥99.5% purity) and sodium chloride, NaCl, (≥99% purity) were purchased from Sigma-Aldrich to purify the obtained DPA. Aniline (99.5% purity) was purchased from Sigma-Aldrich. Ammonium persulfate - APS, $(NH_4)_2S_2O_8$, (≥99.5%, Aldrich) was used for stabilizing the emulsion systems and synthesis of polyaniline. All chemicals were used as received without any further purification. Deionized water was used for the synthesis and purification.

2. Synthesis of Decyl Phosphonic Acid

Michaelis-Arbuzov and Michaelis-Becker reactions are the most used for the synthesis of phosphonate compounds [5,17,20]. In the present case, the synthesis of DPA was realized through two stages, i.e. Michaelis-Arbuzov reaction followed by the hydrolysis of phosphonate ester to obtain the final product (Fig. 1).

2-1. Synthesis of Diethyl Decyl Phosphonate (Stage 1)

Triethyl phosphite (15 mL, 0.087 mol) and decyl bromide (5 mL, 0.024 mol) were added to a 100 mL three-neck round-bottom flask and refluxed at 150 °C for 24 h. A stream of nitrogen bubbles was used to remove the oxygen in the reaction mixture. The reaction mixture was first cooled to room temperature followed by the addition of 55 mL deionized water and finally stirred for 3 h. Next, the mixture was extracted with 40 ml of chloroform. The organic phase containing diethyl decyl phosphonate was purified with 20 ml of brine, and then they were dried with $MgSO_4$. The filtered solution was concentrated by rotary evaporation to give 6.615 g of crude diethyl decyl phosphonate, with very high yield of 99%, as yellow oil.

2-2. Hydrolysis of Phosphonate Ester to Obtain DPA (Stage 2)

Diethyl decyl phosphonate obtained in stage 1 was added to a 500 mL three-neck round-bottom flask containing 200 mL of concentrated HCl solution. The reaction mixture was heated at 100 °C for 12 h with reflux condenser and under nitrogen atmosphere. After the reaction, the mixture was cooled to get crystallized DPA, filtered and washed several times with acetonitrile to remove impurities before it was re-crystallized from petroleum ether to give 4.559 g of pure DPA (yield of 87%).

3. Preparation of Emulsion Systems and Polyaniline Nanoparticles

3-1. Oil-in-Water (O/W) Emulsion

0.694 g (3.125 mmol) of DPA was dissolved in 330 mL of deionized water to form an O/W emulsion. To facilitate of DPA dissolution, the aqueous phase was heated to 55 °C under constant stirring to obtain a homogeneous solution. To improve the stability of the emulsion, 0.357 g of APS (1.563 mmol) was added to the obtained mixture.

3-2. Water-in-Oil (W/O) Emulsion

A W/O emulsion was prepared by dispersing DPA (0.694 g, 3.125 mmol) in 300 mL of *n*-heptane-chloroform mixture (v/v=2/1) and 30 mL of deionized water. The mixture was sonicated for 2 h to obtain a milky system. The milky white emulsion would rapidly separate into the two phase if the emulsion was rested without stirring. The addition of 0.357 g of APS (1.563 mmol) to this system also helps to improve the stability of W/O emulsion.

3-3. Polyaniline Nanoparticles

Polyaniline (PANI) nanoparticles were prepared by the same methods as described by Perrin et al. [22,23]. Following these methods, aniline (1.563 mmol) was added in the O/W and W/O emulsion systems to obtain PANI-OW and PANI-WO.

4. Preparation of Adsorption Layers on Metal Surface and PANI-containing Coatings

Mild steel plates (12.7 cm×7.6 cm×0.08 cm, Labomat) were sand blasted to obtain a surface roughness (R_z) of 20-25 μm, then de-

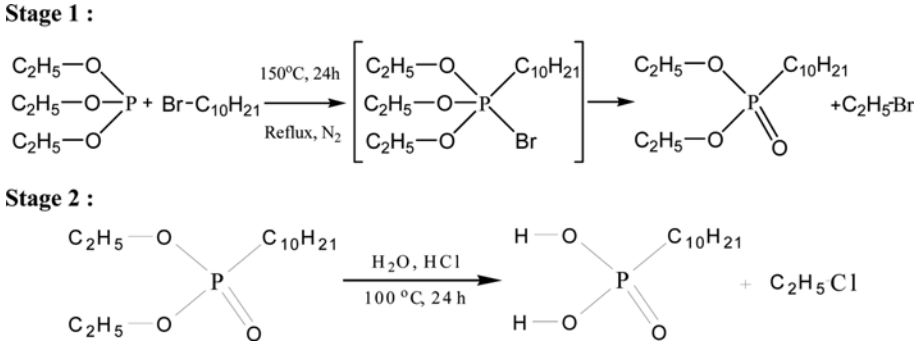

Fig. 1. Reaction pathway of DPA synthesis.

greased with acetone and dried in nitrogen stream. The adsorption layers on mild steel surface were produced by liquid phase reaction. The DPA solution (0.1 wt%) was prepared by dissolving DPA powder into ethanol with agitation for 15 min. Sanded mild steel substrate was immersed into DPA solution at room temperature for 24 h and then rinsed several times with fresh solvent and sonicated to remove physisorbed molecules. Sample rinsed in ethanol was dried carefully in a stream of nitrogen gas. The DPA coated mild steel substrate was covered by the solution of Polyvinyl Butyral, PVB, 15% w/w in ethanol, using a bar coater to obtain DPA/PVB two-layer coating. The sanded mild steel plate was coated with the neat Polyvinyl Butyral, PVB, which was used as a control sample.

Coatings containing 2 wt% of PANI-OW and PANI-WO were prepared according to the procedure described by Perrin et al. [22,23].

5. Corrosion Resistance Testing

The coatings were dried in air at ambient temperature for 24 h followed by drying in an oven at 50 °C for 12 h. The thickness of coatings was 25±3 μm, which was determined by micrometer screw gauge (Elcometer 456/3). The EIS technique was used to evaluate the anti-corrosion properties of the developed coatings during immersion in solution of 3.5% NaCl by using a potentiostat EGG PAR 273 A coupled with a 1255 Solartron frequency response analyzer. The EIS measurements were performed over the frequency range from 20 mHz to 100 kHz with an amplitude sinusoidal perturbation of 10 mV rms. A conventional three-electrode system was used with the saturated calomel electrode (SCE) as reference, the platinum foil as the counter electrode, and the coated metal (~15.7 cm^2 of exposed area) as working electrode. Zview software (Scribners Associates, USA) was used to register and analyze the data of EIS. The coatings were artificially scratched with a vertical scribe of 1 mm×50 mm. Salt-spray corrosion tests were realized according to the ASTM B117 Standard.

6. Characterization of DPA

6-1. Nuclear Magnetic Resonance Spectroscopy

The chemical structure was characterized by ^1H and ^{13}C-NMR spectroscopy. NMR spectroscopy was carried out on a Brüker Avance 400 spectrometer operating at 400 MHz using chloroform-d ($CDCl_3$) as solvent. The spectra were referenced to the solvent signal ($\delta(^1H)$=7.26 ppm and $\delta(^{13}C)$=77 ppm).

6-2. Infrared Spectroscopy

Thermo Nicolet NEXUS instrument was used to record FTIR spectra. Samples were mixed with KBr and further compressed into pellets for measurements. The infrared spectra were obtained for 64 scans and resolution of 4 cm^{-1} in the region between 4,000 and 400 cm^{-1}.

6-3. Differential Scanning Calorimetry Analysis

The thermal transition of DPA was followed by the DSC using a DSC Q10 (TA Instruments, USA) in nitrogen atmosphere (50 mL min^{-1}) from 30 °C to 150 °C at scan rate 10 °C min^{-1}. The thermal transitions were evidenced by the peak maxima in the second heating curve using Universal Analysis 2000 software.

6-4. Thermogravimetric Analysis

TGA was performed using a TA Instrument apparatus (TGA Q600). The sample was heated up to 800 °C with a rate of 10 °C min^{-1} in 100 mL min^{-1} nitrogen. All the samples were analyzed in powder form.

6-5. X-ray Diffraction (XRD)

XRD patterns of synthesized DPA powder were performed with a Siemens® D5000 X-ray diffractometer equipped with a Ni-filtered Cu K_α (λ=0.154 nm) radiation source at 45 kV and 35 mA. The detector scanned from 3° to 40° with step ($\Delta 2\theta$=0.04°) at a scanning speed of 0.002° s^{-1}.

6-6. Dynamic Light Scattering

Micelles sizes (expressed as z-average values) and zeta potential were measured using a zetananosizer (model ZS, Malvern Instrument) at a scattering angle of 173° and 25 °C. The log-normal size distribution was used to evaluate the polydispersity index (PDI). Emulsion samples were prepared by diluting 40 μL of O/W emulsion in 1.2 mL of deionized water and 0.5 mL of W/O emulsion in 0.5 mL of n-heptane.

6-7. Water Contact Angle Measurements

Prior to contact angle measurement, steel substrates were treated via the process described in Section 2.4. All the contact angle measurements were performed at room temperature using a sessile drop method with a DIGIDROP contact angle meter from GBX Instruments. Distilled water droplets of about 1 μL in volume were gently deposited on the surface of DPA absorbed steel sample by using a micro-syringe. A non-treated steel sample was used as a reference for evidencing the effect of DPA on interfacial tension properties. Obtained images of the contact angles were analyzed using Windrop software.

RESULTS AND DISCUSSION

1. Chemical Structure and Purity of Synthesized DPA Product

1-1. Nuclear Magnetic Resonance Spectroscopy

Chemical structure of synthesized DPA was confirmed by ^1H NMR and ^{13}C NMR in $CDCl_3$. The obtained results are shown in Fig. 2 and Fig. 3, respectively.

The peaks at a, b, c, d, e, f and a′, b′, c′, d′, e′, f′, g′ on the NMR spectra are attributed to different protons and carbon atoms in the DPA chemical structure, respectively. The chemical shifts, the number of signals, the signals splitting and their integration intensity revealed that the chemical structure of DPA was perfectly consistent with that in literature [20,21]. Moreover, NMR results confirm

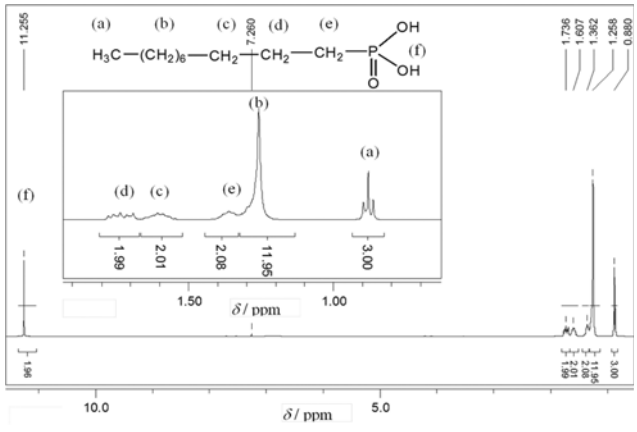

Fig. 2. ^1H NMR spectra of DPA in $CDCl_3$.

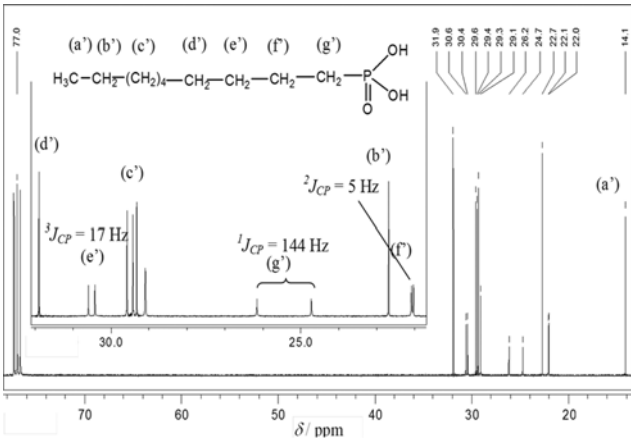

Fig. 3. ^{13}C NMR spectra of DPA in $CDCl_3$.

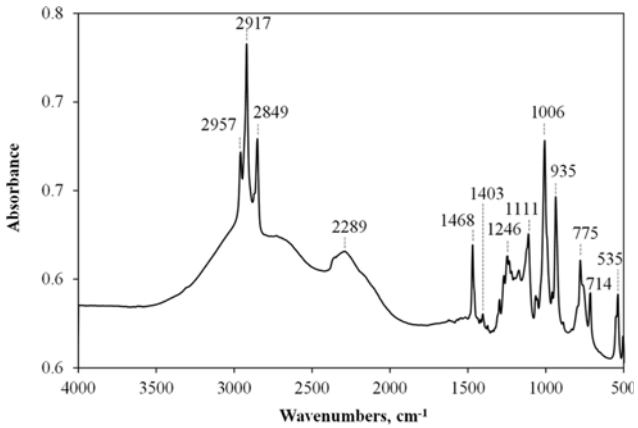

Fig. 4. FTIR spectra of DPA product.

the high purity of DPA product.

1-2. Infrared Spectroscopy

Fig. 4 shows the infrared spectrum of DPA powder. The C-H stretching vibrations of the methylene group are often present in the frequency region from 2,800 cm^{-1} to 3,000 cm^{-1}. Position of the methylene group in the infrared spectrum can be used to determine the ordering of the alkyl chain [4,24-26]. For disordered chains, the position of the CH_2 stretching is close to that of a liquid alkane ($\nu_{CH2asym}$~2,924 cm^{-1}) due to the presence of gauche conformations in the alkyl chains [26]. For well-ordered alkyl chains, the position is shifted to lower wavenumbers and is close to that of a crystalline alkane ($\nu_{CH2asym}$~2,914-2,918 cm^{-1}) which is considered to have a high degree of order. In this study, the positions of peaks corresponding to $\nu_{CH2asym}$ and ν_{CH2sym} were 2,917 cm^{-1} and 2,849 cm^{-1}, which indicates that DPA has all-trans conformations throughout the alkyl chain. The absorption bands at 1,468 and 1,403 cm^{-1} are attributed to the scissoring mode (δ) of C-H bond. The P-OH groups have two broad absorption bands of weak to medium intensities in the regions 2,700-2,500 cm^{-1} and 2,300-2,100 cm^{-1}, which are due to the O-H stretching vibrations [9]. These broadened and weak absorption bands are also characteristics for hydrogen bonding between P-OH groups. The strong absorption band in the region of 1,250-1,150 cm^{-1} is attributed to the stretching vibration of the P=O group [9,17,27]. The absorption bands of medium to strong intensity at 1,040-910 cm^{-1} are associated with the P-O stretching vibrations [4]. The absorption bands at 775 cm^{-1} and 714 cm^{-1} are attributed to the rocking vibrational mode (γ) of CH_2 group and the stretching vibrational mode of P-C group [21,28].

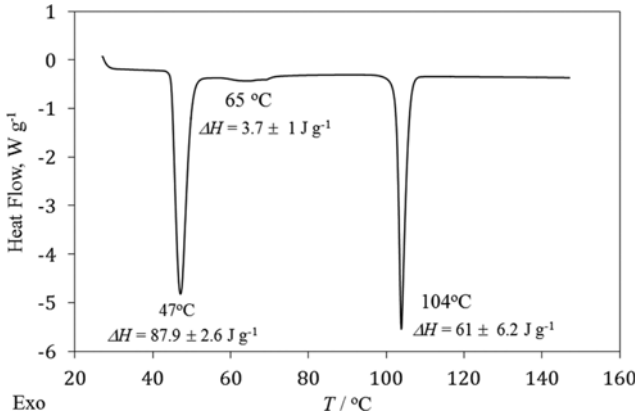

Fig. 5. DSC curve of DPA.

2. Thermal Properties of DPA Product

2-1. Differential Scanning Calorimetry Analysis

As shown in Fig. 5, there are three thermal transitions appearing in the DSC curve of DPA (in the temperature range from 30 to 140 °C).

The first transition takes place at 47 °C with an enthalpy of ΔH= 87.9±2.6 J g^{-1}. This transition can be attributed to a partial "melt" of the hydrocarbon chains that caused a slight change in the structure and in the polar hydrogen bonded network. However, the external shapes of DPA crystals are not changed because the hydrogen-bonded network is still strong enough to maintain the rigid structure of DPA. Below the first thermal transition, DPA crystals were transparent, if they were crystallized from aqueous or organic solution [29]. The second transition appears at 65 °C with an enthalpy of ΔH=3.7±1 J g^{-1}. This transition could be explained by the total melting of the hydrocarbon chains. Also at this temperature, the hydrogen bonds at the polar bilayer become dynamic. The result of this process is the appearance of a visco-isotropic (cubic) mesophase. On the DSC curve, the third transition is observed at 104 °C with ΔH=61±6.2 J g^{-1} which corresponds to the melting of the cubic liquid crystal to become isotropic liquid phase [27,29].

2-2. Thermogravimetric Analysis

TGA curves (Fig. 6) show the main decomposition of DPA product at around 400 °C in air as well as in nitrogen atmosphere.

While the thermal decomposition of DPA in nitrogen occurred only in one step at 428 °C, three different decomposition steps at 411, 446 and 576 °C were observed for the decomposition in air. In nitrogen, only 1.7 wt% remained at 440 °C, which indicated that the DPA was decomposed almost completely. This result is quite comparable to those in previous studies [30,31]. In the air, the weight loss between 411 and 446 °C is attributed the main decomposition of alkyl groups to methylene and methyl groups. The weight loss at around 576 °C might be due to the degradation of polar head groups. In this temperature range, the condensation of phosphoric acid to polyphosphate may occur via the cross-linking of P-O-P to

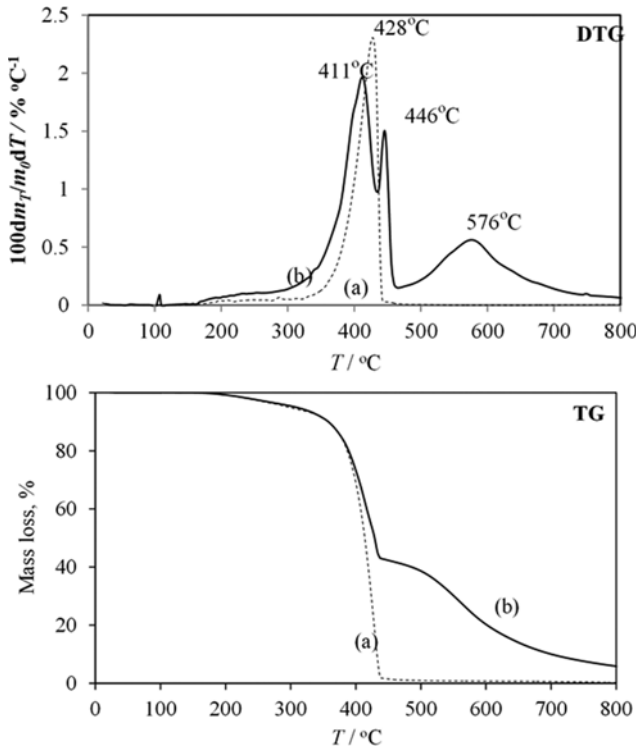

Fig. 6. Thermal decomposition of DPA: (a) In nitrogen, (b) in the air.

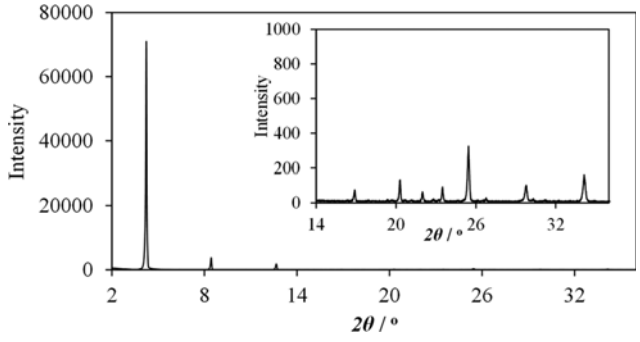

Fig. 7. X-ray diffraction pattern of DPA.

form the non-combustible residues [30-32]. At 800 °C, the residue was 6.3%, which could be belonging to phosphorus compounds [30].

3. Crystal Structure of DPA Product

The XRD patterns of DPA are shown in Fig. 7. The diffraction peaks in the low-angle region of the XRD pattern are characteristics of highly ordered structures. In the case of DPA, the formation of a well-organized layered structure is due to the effect of the complex system of hydrogen bonds between -PO_3H_2 groups. The distance between these layers is about 21.6 Å corresponding to a diffraction at 2θ=4.1° [21]. The interlayer interactions are of the very weak van der Waals type. Two peaks at 2θ=8.2° (d=10.8 Å) and 2θ=12.3° (d=7.2 Å) could be attributed to the diffractions between ordered bundles in the long chain alkyl structure. A low-intensity peak was observed at 2θ=20.2° corresponding to d=4.4 Å, which is attributed to the distance between the carbon atoms of

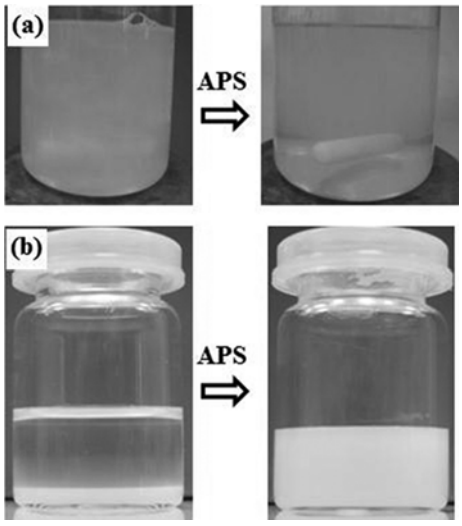

Fig. 8. Formation of O/W emulsion (a) and W/O emulsion (b).

Table 1. Micelles size, zeta potential (ξ) and pH of emulsion when change of DPA concentration

[DPA] (mM)	Size (nm)	PDI	Zeta potential (mV)	pH
O/W emulsion				
3.79	268	0.41	−55	3.12
5.68	325	0.23	−58	3.01
9.47	340	0.26	−64	2.98
18.94	408	0.34	−58	2.80
W/O emulsion				
9.47	188	0.11	-	-
18.94	210	0.14	-	-
28.41	225	0.16	-	-
37.88	232	0.2	-	-

the neighboring hydrocarbon chains. The alkyl chains in the crystal of DPA have the all-trans conformation [21].

4. Interfacial Tension Properties of DPA as Surfactant

The interfacial tension properties of DPA were investigated. At concentrations above the critical micelle concentration (cmc=1.66 mM [27]), the DPA molecules aggregate to form the micelles. In O/W emulsion, the DPA molecules tended to form vesicles rather than micelles [33] while the micelles with core consisting of discrete spherical water droplets and shell consisting of monolayer of surfactant were found in the W/O emulsion [23]. The formation of DPA vesicles made the O/W emulsion system become turbid, but the mixture became more transparent with the addition of APS. Similarly, as can be seen in Fig. 8, the addition of APS helped to improve the stability of the W/O emulsion significantly [23]. The stabilization effect of APS may be related to the selective adsorption of persulfate ion on the micelles surface leading to repulsive interactions between the DPA micelles. The larger the repulsive interactions, the smaller the micelle sizes.

DLS is an efficient technique to determine the size and size distribution of micelles [34]. The micelle size, zeta potential (ξ) and

pH of emulsions are summarized in Table 1. The size of micelles in O/W emulsion, expressed as z-average diameter, increases from 270 to 400 nm with an average polydispersity index (PDI) of 0.31± 0.08 when the DPA concentration increases from 3.79 to 18.94 mM. For the W/O emulsion, the size of micelles is established around 240 nm with PDI less than 0.2 (0.16±0.03). The results indicate that the W/O emulsion is a monodisperse system. The zeta potential in O/W emulsion varies from −55 to −65 mV, which guarantees a high stability of the O/W emulsion system. As the pH of emulsion decreases when increasing DPA content, it is reasonable to suppose that along with the selective persulfate adsorption, the negative zeta potential value is generated by partial ionization of DPA acid groups on the surface. This is an advantage when the DPA is used as a surfactant.

5. Wetting Properties

The orientation of the DPA molecules in the adsorbed layer on metal surface can be easily determined by the water contact angle measurement; this method was thus used to evaluate the wetting properties of DPA. The DPA molecules with ten-carbon chain are long enough to provide mobility for the formation a well-organized structure containing all-trans configuration throughout the alkyl chain. The presence of all-trans configuration in the adsorbed layer is evidenced by the appearance of antisymmetric C-H stretching mode at 2,918 cm^{-1} and symmetric C-H stretching mode at 2,852 cm^{-1} in the IR spectra as shown in Fig. 9.

On the mild steel substrate, the DPA furthermore formed a well-ordered film which cannot be removed by rinsing with ethanol under sonication. On the DPA coated mild steel substrate, the terminal methyl groups of the alkyl chain are oriented outward, reducing access of water droplets to the metal surface. As a result, the water contact angle value obtained on the substrate coated with DPA reaches a value of 114° compared to 60° on uncoated substrate as shown in Fig. 10.

6. Anti-corrosion Performance

For corrosion resistance testing, the developed coatings were exposed to salt in a spray chamber following the standard ASTM standard B117. Fig. 11 shows some images of the developed coatings after 15 days of the corrosion test.

The DPA/PVB two-layer coating and PVB coatings containing DPA doped PANI (PANI-WO and PANI-OW) show better corrosion protection performance than the pristine PVB coating as evidenced by fewer corrosion products accumulated in the scribe. At the end of the salt spray tests, the PVB topcoat was carefully detached in ethanol using a stiff brush to evaluate scribe creep corrosion. The creep corrosion process is less observed in the DPA/PVB two-layer coating and PVB coatings containing DPA doped PANI samples than in the pristine PVB coating one. These results could be at-

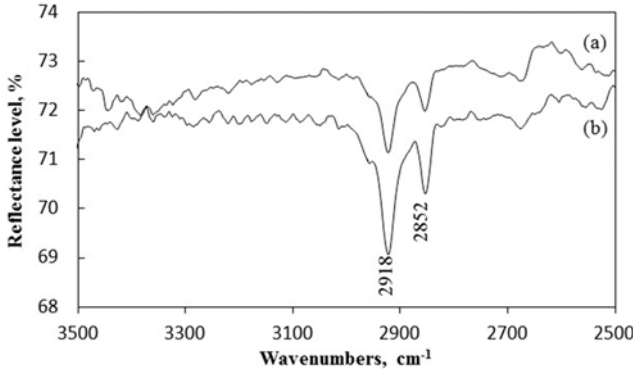

Fig. 9. Infrared reflection spectra of DPA on mild steel substrate after deposition (a) and after rinse (b).

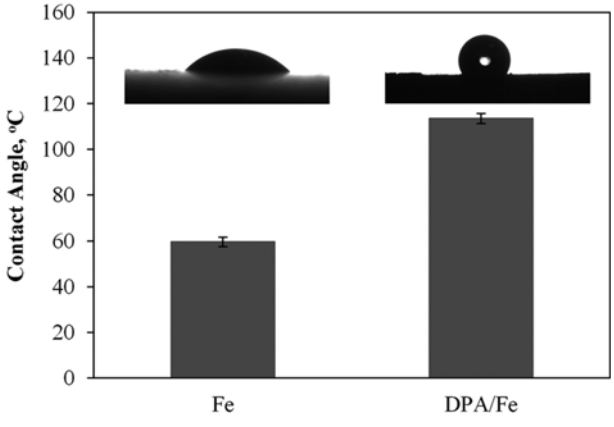

Fig. 10. Contact angles of Fe and DPA/Fe.

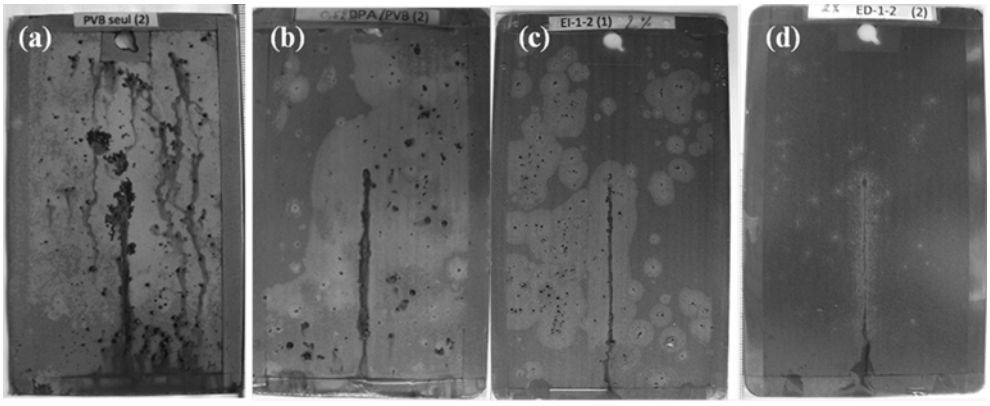

Fig. 11. Optical photos after 360 h of salt spray test: pristine PVB coating (a), DPA/PVB two-layer coating (b), PVB coating loaded with 2 wt% PANI-WO (c), PVB coating loaded with 2 wt% PANI-OW.

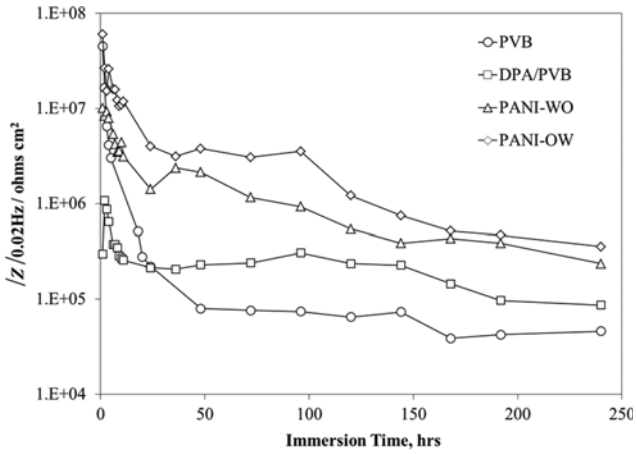

Fig. 12. Evolution of the low frequency impedance with immersion time in 3.5 wt% NaCl solution.

tributed to the inhibiting effect of DPA as well as the hydrophobic nature of DPA adsorption layer. However, when DPA is applied directly as a primer layer, it can prevent the adhesion of PVB topcoat to the substrate surface. As a result, it decreases the corrosion resistance ability of the DPA/PVB two-layer coating compared to the PVB coatings containing DPA doped PANI. Interestingly, the anti-corrosion efficiency of the PVB coating containing PANI-OW is higher than that of the PVB coating containing PANI-WO. This can be explained by the higher DPA content in PANI-OW than in PANI-WO [22,23].

The EIS technique was used to determine the protective performance of the coating in neutral 3.5 wt% NaCl solution. The impedance modulus at low frequency, 20 mHz, characterized the total resistance of the system, a suitable parameter used to determine the anti-corrosion properties of a coating. The impedance modulus at low frequency ($|Z|_{0.02\,Hz}$) consisted of solution resistance (R_s), pore resistance (R_p) and charge-transfer resistance (R_{ct}). Fig. 12 shows that the PVB coating loaded with 2 wt% PANI-OW has the highest impedance modulus values at low frequency, and thus offered the best corrosion protection performance for steel.

CONCLUSION

DPA was successfully synthesized by a two-stage reaction, namely, the Michaelis - Arbuzov reaction followed by a hydrolysis reaction. A very high yield (up to 87%, twice larger than that of previous studies) and a very pure DPA (evidenced by FTIR and NMR spectroscopy) can be obtained. Other properties of DPA such as thermal properties and crystal structures were also determined. Notably, the interfacial tension characteristics of DPA in O/W and W/O emulsion were investigated, and also the effect of APS for enhancing the stability of DPA emulsion systems was proven. The appropriate wetting and good corrosion-inhibition properties of DPA make it a potential candidate for anti-corrosion paint composition.

ACKNOWLEDGEMENTS

The authors gratefully acknowledge Agence Universitaire de la Francophonie (AUF) for the financial support and the Matériaux Polymères Interfaces Environnement Marin (MAPIEM) laboratory for measurements. The first author also acknowledges the Funds for Science and Technology Development of the University of Danang for funding the research project under grant number B2016-ĐN02-01.

REFERENCES

1. A. Kalir and H. H. Kalir, In *PATAI'S Chemistry of Functional Groups*, Wiley (2009).
2. K. Chruszcz, M. Barańska, K. Czarniecki and L. M. Proniewicz, *J. Mol. Struct.*, **651**, 729 (2003).
3. A. F. O. Regina Luschtinetz, *Surf. Sci.*, **602**, 1347 (2008).
4. R. Quiñones, A. Raman and E. S. Gawalt, *Thin Solid Films*, **516**, 8774 (2008).
5. T. Vallant, H. Brunner, U. Mayer and H. Hoffmann, *Langmuir*, **14**, 5826 (1998).
6. I. Maege, E. Jaehne, A. Henke, H.-J. P. Adler, C. Bram, C. Jung and M. Stratmann, *Macromol. Symp.*, **126**, 7 (1998).
7. J. J. Hickman, D. Ofer, P. E. Laibinis, G. M. Whitesides and M. Wrighton, *Science*, **252**, 688 (1991).
8. C. Bressy-Brondino, B. Boutevin, Y. Hervaud and M. Gaboyard, *J. Appl. Polym. Sci.*, **83**, 2277 (2002).
9. I. Maege, E. Jaehne, A. Henke, H.-J. P. Adler, C. Bram, C. Jung and M. Stratmann, *Prog. Org. Coat.*, **34**, 1 (1997).
10. A. Badia, R. B. Lennox and L. Reven, *Acc. Chem. Res.*, **33**, 475 (2000).
11. T. Nakamoto, M. Katada, K. Endo and H. Sano, *Polyhedron*, **17**, 3507 (1998).
12. S. Valiyaveettil, V. Enkelmann and K. Müllen, *J. Chem. Soc. Chem. Commun.*, **18**, 2097 (1994).
13. T. T. Foster, M. R. Alexander, G. J. Leggett and E. McAlpine, *Langmuir*, **22**, 9254 (2006).
14. M. Green and R. F. Hudson, *J. Chem. Soc.*, 3129 (1958).
15. G. M. Kosolapoff, *Organic phosphorus compounds, Vol. 4*; Wiley-Interscience, New York (1972).
16. G. M. Kosolapoff, *Organic Phosphorus Compounds*, *Vol. 7*, 7th Ed., Maier, L., Ed., Wiley, New York (1976).
17. P. Fiurasek and L. Reven, *Langmuir*, **23**, 2857 (2007).
18. Y. Sahoo, H. Pizem, T. Fried, D. Golodnitsky, L. Burstein, C. N. Sukenik and G. Markovich, *Langmuir*, **17**, 7907 (2001).
19. J. K. Thottathil, Process for preparing phosphonic acids, *Patent US* No. 4670193, June 2 (1987).
20. H. S. O. Chan, S. C. Ng and P. K. H. Ho, *Macromolecules*, **27**, 2159 (1994).
21. D. Boczula, A. Cały, D. Dobrzyńska, J. Janczak and J. Zoń, *J. Mol. Struct.*, **1007**, 220 (2012).
22. F. X. Perrin, T. A. Phan and D. L. Nguyen, *Eur. Polym. J.*, **66**, 253 (2015).
23. F. X. Perrin, T. A. Phan and D. L. Nguyen, *J. Polym. Sci. Part Polym. Chem.*, **53**, 1606 (2015).
24. D. L. Allara and R. G. Nuzzo, *Langmuir*, **1**, 45 (1985).
25. R. G. Snyder, H. L. Strauss and C. A. Elliger, *J. Phys. Chem.*, **86**, 5145 (1982).
26. R. Helmy and A. Y. Fadeev, *Langmuir*, **18**, 8924 (2002).

27. P. C. Schulz, M. Abrameto, J. E. Puig, F. A. Soltero-Martínez and A. Gonzalez-Alvarez, *Langmuir*, **12**, 3082 (1996).
28. S. C. D'Andre and A. Y. Fadeev, *Langmuir*, **19**, 7904 (2003).
29. C. C. Schulz, *E-Gnos.*, **1**, 14 (2003).
30. T. Hoffmann, P. Friedel, C. Harnisch, L. Häußler and D. Pospiech, *J. Anal. Appl. Pyrolysis*, **96**, 43 (2012).
31. B. Lafitte and P. Jannasch, *J. Polym. Sci. Part Polym. Chem.*, **43**, 273 (2005).
32. D. D. Jiang, Q. Yao, M. A. McKinney and C. A. Wilkie, *Polym. Degrad. Stab.*, **63**, 423 (1999).
33. P. Walde, M. Wessicken, U. Rädler, N. Berclaz, K. Conde-Frieboes and P. L. Luisi, *J. Phys. Chem. B*, **101**, 7390 (1997).
34. E. B. Leodidis and T. A. Hatton, *Langmuir*, **5**, 741 (1989).